Journal of Applied Polymer Science

Structural Characterization of Hydrophilic Polymer Blends/ Montmorillonite Clay Nanocomposites

Ram Jeewan Sengwa, Shobhna Choudhary
Department of Physics, Dielectric Research Laboratory, Jai Narain Vyas University, Jodhpur 342 005, India
Correspondence to: R. J. Sengwa (E-mail: rjsengwa@rediffmail.com)

ABSTRACT: The nanocomposite films comprising polymer blends of poly(vinyl alcohol) (PVA), poly(vinyl pyrrolidone) (PVP), poly(ethylene oxide) (PEO), and poly(ethylene glycol) (PEG) with montmorillonite (MMT) clay as nanofiller were prepared by aqueous solution casting method. The X-ray diffraction studies of the PVA–*x* wt % MMT, (PVA–PVP)–*x* wt % MMT, (PVA–PEO)–*x* wt % MMT and (PVA–PEG)–*x* wt % MMT nanocomposites containing MMT concentrations $x = 1$, 2, 3, 5 and 10 wt % of the polymer weight were carried out in the angular range (2θ) of 3.8–30°. The values of MMT basal spacing d_{001}, expansion of clay gallery width W_{cg}, *d*-spacing of polymer spherulite, crystallite size *L* and diffraction peak intensity *I* were determined for these nanocomposites. The values of structural parameters reveal that the linear chain PEO and PEG in the PVA blend based nanocomposites promote the amount of MMT intercalated structures, and these structures are found relatively higher for the (PVA–PEO)–*x* wt % MMT nanocomposites. It is observed that the presence of bulky ester-side group in PVP backbone restricts its intercalation, whereas the adsorption behavior of PVP on the MMT nanosheets mainly results the MMT exfoliated structures in the (PVA–PVP)–*x* wt % MMT nanocomposites. The crystallinities of the PEO and PEG were found low due to their blending with PVA, which further decreased anomalously with the increase of MMT concentration in the nanocomposites. The decrease of polymer crystalline phase of these materials confirmed their suitability in preparation of novel solid polymer nanocomposite electrolytes.
 J. Appl. Polym. Sci. **2014**, *131*, 40617.

KEYWORDS: blends; clay; composites; hydrophilic polymers; X-ray

Received 2 November 2013; accepted 17 February 2014
DOI: 10.1002/app.40617

INTRODUCTION

In the advancement of materials science and technology, the polymer–clay nanocomposites (PCNs) have emerged as a new class of materials for the academic, industrial, and technological interest.[1–14] Most of the studies have documented that the formation of the intercalated and exfoliated clay structures in the polymer matrix have resulted in the improvement of the thermal (increased heat resistance and reduced flammability) and mechanical properties of the host polymer matrix.

In past two decades, the PCNs consisted of different polymers with a variety of clays as nanofiller were prepared by different methods, and their performance properties were characterized by the advanced spectroscopic and mechanical techniques. Among the synthetic polymers, poly(vinyl alcohol) (PVA), poly(vinyl pyrrolidone) (PVP), poly(ethylene oxide) (PEO), and poly(ethylene glycol) (PEG) are hydrophilic and biodegradable polymers, which have a large technological and pharmaceutical applications.[15] These polymers have good solubility in water due to the formation of strong hydrogen bond (H-bond) between the functional group of polymer and the water molecules. The aqueous solutions of PVA, PVP, PEO and PEG form the complexes with the additives/dopants, which make them technological important as binder material. Further, these polymers have good film forming ability when the polymeric films are prepared by solution casting technique. The films of the PVA and the PVP are highly optically transparent, which makes them suitable for surface coating of the solid state optoelectronic devices and other multifunctional materials. The functional groups of these polymers have strong affinity to form the ion-dipolar interactions with the alkali metal salts. These interactions can dissociate the alkali salt up to high degree. Therefore these polymers are extensively used in preparation of flexible, light weight and safe type solid polymer nanocomposite electrolytes (SPNEs).[16–23] The SPNEs find large applications in the advancement of the lithium ion battery technology and also in the design of ion conduction dependent electrochromic devices.[16–23] The main drawbacks of the hydrophilic polymers are their poor mechanical and thermal stability. For the improvement in these performance properties, the preparation and

characterization of the hydrophilic polymer based PCNs are in progress.[4,5,12–14]

The montmorillonite (MMT) clay is frequently used for the preparation of PCNs, because of its hydrophilic behavior identical to the organic polymers.[24] The MMT has 2 : 1 charged phyllosilicate sheets of 1 nm thickness and these are stacked by weak dipolar or van der Waals forces. Due to presence of interlayer spacing between the stacked MMT nanosheets, they have a large swelling behavior and the compatible interactions especially with the hydrophilic polymers which result the intercalated and exfoliated structures of the PCNs. The proper dispersion of clay in the polymer matrix with a state-of-the-art is also important for the successful development of good quality PCN materials with their tailored properties.

The preparation and characterization of the nanocomposites based on the clay with PVA,[25–31] PVP,[32–38] PEO,[39–51] and PEG[52–56] have been subject of intense investigations. The outcomes of various studies on these materials have established that the dispersion of MMT in the PVA, PVP, PEO, and PEG matrices improves their mechanical, thermal, gas permeable and dielectric/electrical properties. The research work on the PVA blends with PVP,[57–67] PEO,[68–70] and PEG[71–73] also confirms the enhancement in their technological and industrial important physicochemical properties as compared with the individual polymer. These improved properties of the polymers blends depend on the miscibility and the heteromolecular interaction compatibility generated between the functional groups of the polymers. The bridging of homo and hetero polymers chains in presence of inorganic nanofillers also plays a major role in tailoring the required properties of the polymers blend based composite materials. Our survey of literature reveals that the detailed structural parameters and the crystallinity of nanocomposites consisted of PVA–PVP, PVA–PEO and PVA–PEG blends with varying concentration of MMT nanofiller have not been explored so far. The scarcity of fine structural parameters impedes further advancement of industrial applications of these PCN materials.

In the last few years, authors have prepared the PCN colloids and films based on the PVA–PVP, PVA–PEO, and PVA–PEG blends with MMT nanofiller, and their detailed dielectric/electrical properties and the molecular dynamics were characterized using the dielectric relaxation spectroscopy (DRS).[33,51,74–77] The effect of MMT concentration on the electrical behavior and the polymer chain segmental dynamics of these materials was characterized in view of their suitability as novel flexible type dielectric/insulator material for the fabrication of microelectronic devices. In continuation of our earlier work on these nanocomposite materials, in this article an attempt has been made to reveal the detailed structural parameters and crystallinity of the PCNs comprising PVA and its blends with the PVP, PEO, and PEG as a function of MMT nanofiller concentration by X-ray diffraction (XRD) measurements. In preparation of polymers blends, the PVA weight used is three times as compared with the weight of the PVP, PEO, and PEG. The higher amount of PVA has been kept in the blend because the PVA film has relatively high optical transparency, flexibility, and the mechanical stability. Therefore, such type of polymer blend nanocomposites can prove their suitability as the binder and the novel dielectric materials in the optoelectronic technology, besides their use in preparation of the advanced SPNE materials.

EXPERIMENTAL

Materials

The PVA ($M_w = 77{,}000$ g mol^{-1}) and PEG ($M_w = 4000$ g mol^{-1}) of laboratory grade were obtained from Loba Chemie, and the PVP ($M_w = 24{,}000$ g mol^{-1}) was obtained from S.D. Fine-Chem, India. The PEO ($M_w = 600{,}000$ g mol^{-1}) and polymer grade hydrophilic montmorillonite (MMT) nanoclay (PGV, a product of Nanocor®) were purchased from Sigma-Aldrich, USA. The MMT is white in colour, and has 145 meq/100 g cation exchange capacity (CEC), 150−200 aspect ratio (length/breadth), 2.6 g/mL specific gravity, and 9−10 pH value on 5% dispersion.

Sample Preparation

The blends of the PVA–PVP, PVA–PEO, and PVA–PEG were prepared at 75 : 25 weight ratios (wt/wt %). The quantity of MMT dispersed in the amount of polymer was expressed as weight percent (x wt % MMT). In the present study, $x = 0$, 1, 2, 3, 5, and 10 wt % MMT were used for the preparation of PVA–x wt % MMT, and (PVA–PVP)–x wt % MMT, (PVA–PEO)–x wt % MMT, and (PVA–PEG)–x wt % MMT nanocomposites. The films of these PCNs were prepared by solution casting method. Initially the aqueous polymeric solutions were prepared by dissolving the required amounts of each polymer in double distilled deionized water in air tight caped glass bottles. After that the polymer solutions were mixed, which resulted the aqueous polymer blend solutions. The amounts of MMT corresponding to each concentration (x wt % MMT) were dispersed in deionized water and allowed to swell by vigorous stirring with the Teflon coated magnetic bar on a magnetic stir plate for 24 h in separate glass bottle. After that various concentration hydrocolloids of MMT were mixed with the respective aqueous polymer blend solutions and these were again vigorously stirred by magnetic bar for 24 h to achieve the homogenous solutions. The homogenously mixed viscous polymer nanocomposite solutions were cast onto Teflon petri dishes of 60 mm diameter and left for drying at room temperature for one week duration, which resulted in the free standing PCN films. These free standing films of the PVA–x wt % MMT, (PVA–PVP)–x wt % MMT, (PVA–PEO)–x wt % MMT and (PVA–PEG)–x wt % MMT nanocomposites were further dried under vacuum at 40°C for 12 h to remove the water traces, if any, before performing their XRD measurements.

XRD Measurements

The XRD patterns of MMT powder, the films of pure polymer, polymer blends, and the polymeric nanocomposites were recorded in reflection mode using a PANalytical X′pert Pro MPD diffractometer of Cu-K_α radiation (1.5406 Å) operated at 45 kV and 40 mA, with a scanning step size of 0.05°/s. The powder sample of MMT was tightly filled in the sample holder, whereas each film was placed on top of the sample holder during the XRD scanning in the angular range $2\theta = 3.8$ to 30°, at

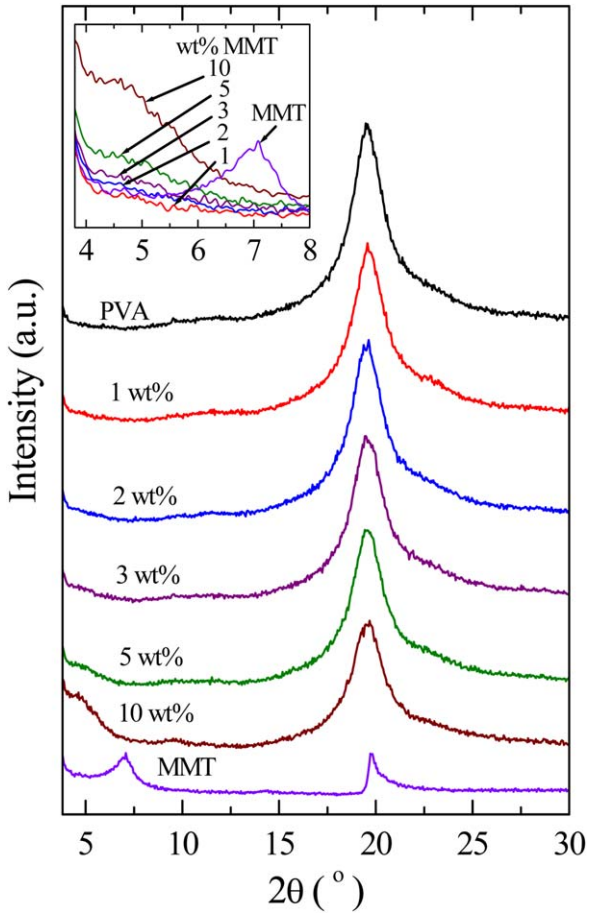

Figure 1. XRD patterns of aqueous solution cast pure PVA and PVA–*x* wt % MMT nanocomposites films, and MMT powder. Inset shows the enlarged view of 001 reflection peak of MMT in the nanocomposites. [Color figure can be viewed in the online issue, which is available at wileyonlinelibrary.com.]

room temperature. Figures 1–4 show the XRD patterns of different nanocomposite materials. For the comparison, these patterns are displaced from one another vertically with change of MMT concentration in the nanocomposites. A series of XRD scans was repeated using some of the samples prepared separately by same procedure, which showed excellent agreement.

The values of crystal reflection peak position 2θ, the peak intensity I (counts) and full width at half maximum FWHM or β (the broadening of peak at half-height expressed in radians of 2θ i.e. width measured in 2θ degrees and then multiplied by $\pi/180$) of the investigated materials were determined by a X'pert pro® software. The values of basal spacing of crystal reflections are determined by the Bragg's relation $\lambda = 2d\sin\theta$, where λ and d are the wavelength of X-ray radiation ($\lambda = 1.5406$ Å) and the spacing between diffraction lattice planes of the crystal, respectively. The values of mean crystallite size L in the direction perpendicular to hkl plane of the polymers and their nanocomposites are determined by Scherrer's equation $L = 0.94\lambda/\beta\cos\theta$. The evaluated values of 2θ, d, L, and I corresponding to the various crystal reflection peaks of the nanocomposite materials are recorded in Tables I–IV.

RESULTS AND DISCUSSION

PVA–x wt % MMT Nanocomposites

Figure 1 shows the XRD patterns of MMT powder, and aqueous solution cast pure PVA and PVA–*x* wt % MMT nanocomposite films. The characteristic features of these patterns are (i) the MMT powder has a peak at $2\theta = 7.03°$ which is corresponding to 001 crystallographic plane of its crystal structure, whereas the other peak at 19.79° represents the 101 crystal reflection plane. These peaks positions are found in good agreement with the earlier studies,[25,30] (ii) the broad peak appeared at 19.56° for aqueous solution cast PVA film confirms the dominance of amorphous component over the crystalline phase in its semi-crystalline structure, and this peak can be attributed to concerted crystal reflection planes $10\bar{1}$,101 of the PVA.[17,25,26,28,30] The decrease in intensity of concerted $10\bar{1}$ and 101 peaks is accompanied by the appearance of a centered broad single peak of the aqueous solution cast PVA film, and (iii) the low intensity peak for PVA–*x* wt % MMT nanocomposites corresponding to 001 reflection plane of MMT is observed at lower Bragg's angle as compared with that of the pure MMT (inset of Figure 1). The intensity value of concerted $10\bar{1}$,101 reflection peak of

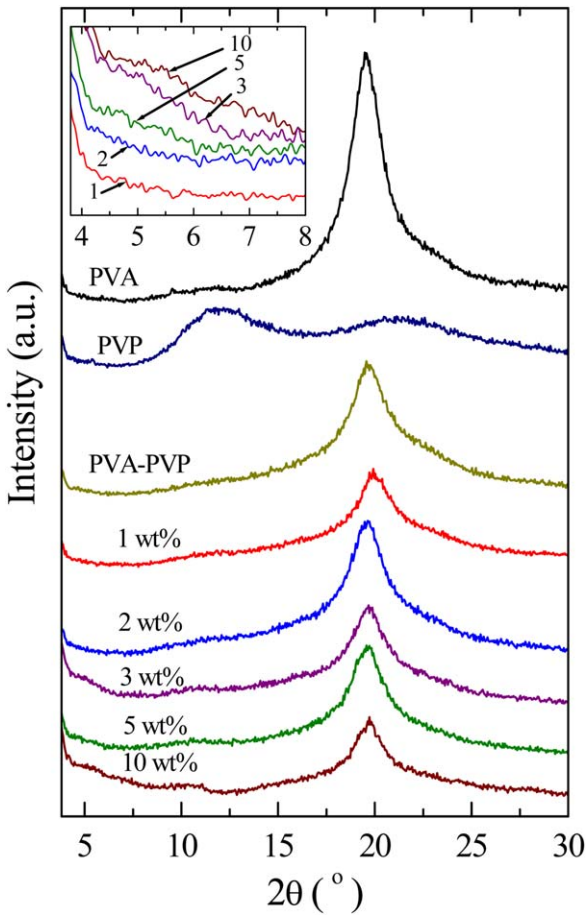

Figure 2. XRD patterns of aqueous solution cast pure PVA, PVP, (PVA–PVP) blend, and (PVA–PVP)–*x* wt % MMT nanocomposites films. Inset shows the enlarged view of 001 reflection peak of MMT in the nanocomposites. [Color figure can be viewed in the online issue, which is available at wileyonlinelibrary.com.]

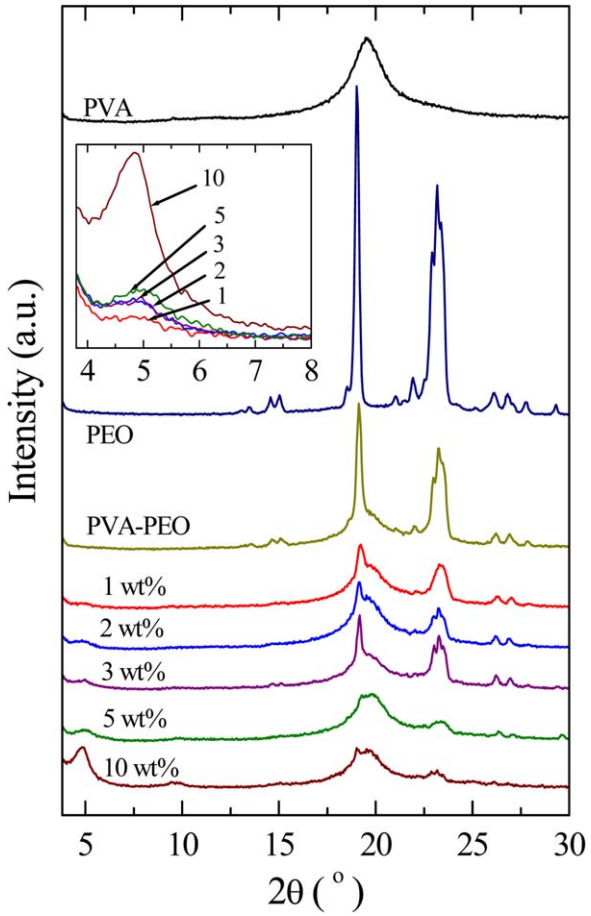

Figure 3. XRD patterns of aqueous solution cast pure PVA, PEO, (PVA–PEO) blend, and (PVA–PEO)–*x* wt % MMT nanocomposites films. Inset shows the enlarged view of 001 reflection peak of MMT in the nanocomposites. [Color figure can be viewed in the online issue, which is available at wileyonlinelibrary.com.]

PVA is found reduced for these nanocomposites. These observations confirm the complexations between MMT and PVA which result in the enhancement of the nanocomposite amorphous phase.[27]

The appearance of 001 crystal reflection peak about 2° lower angle side than that of the pure MMT for the PVA–*x* wt % MMT nanocomposites (2θ values are given in Table I) confirms the formation of MMT intercalated structures. In these structures some amounts of PVA have entered into the MMT interlayer galleries which resulted in the increase of d_{001} spacing. The width of intercalated MMT gallery W_{cg} of the nanocomposites is determined by the relation $W_{cg} = d_{001} - W_{cl}$, where W_{cl} is the clay layer width in *c*-axis, which is 9.6 Å (0.96 nm) for the MMT clay.[56] The W_{cg} value of pure MMT powder is found 0.297 nm, which is due to the presence of hydrated exchangeable cations, mostly the sodium cation Na^+ in the MMT clay. For the PVA–*x* wt % MMT nanocomposites, the W_{cg} values are found in the range of 0.70 to 0.96 nm which confirm that the intercalated PVA has its one or probably two layers planner arranged structures in the MMT galleries. Table I shows that the intensity (counts) I_{001} values corresponding to the MMT crystal 001 peak are very low, and these values also have anomalous increase with the increase of MMT concentration in the nanocomposites. The low I_{001} peak value confirms that the amount of intercalated MMT is very small. It seems that most of the added MMT has the exfoliated structures in these nanocomposites, because the exfoliated MMT in the polymer matrix does not show any crystalline peak.[38] The presence of Na^+ ions in the MMT galleries and their interactions with the –OH groups of PVA promote the intercalation, whereas the MMT silanol (Si–O) interactions with the –OH groups of PVA result in PVA adsorption on the MMT surfaces which lead to increase in amount of MMT exfoliated structures.[77] At 10 wt % MMT, relatively high I_{001} value of the nanocomposite confirms a small increase of the MMT intercalated structures, although this peak intensity value is still low as compared with that of the pure MMT (Table I).

The aqueous solution cast PVA film has around 30% crystalline phase.[78] The XRD parameters of PVA–*x* wt % MMT nanocomposites reveal that loading of MMT in PVA matrix up to 10 wt % has negligible effect on PVA crystal reflection peak position (2θ). Therefore the *d*-spacing values corresponding to concerted

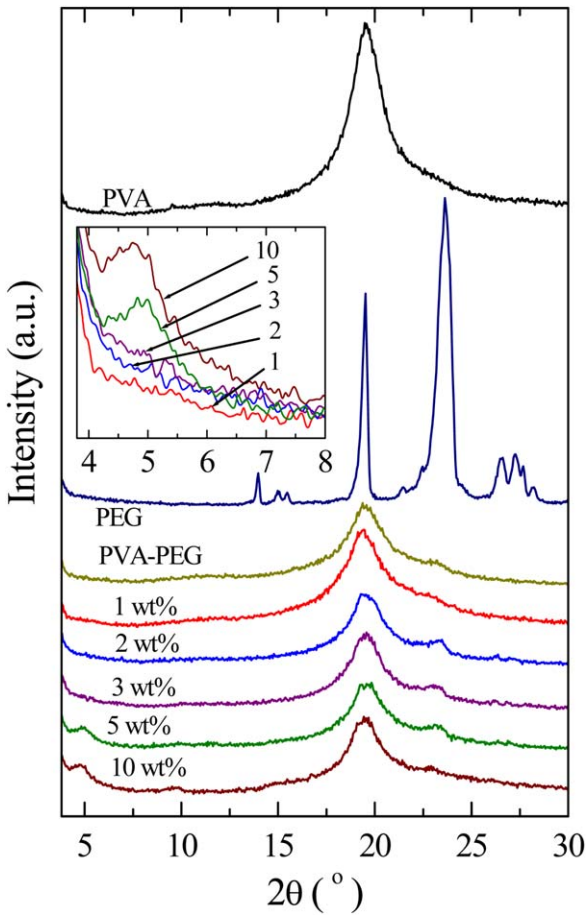

Figure 4. XRD patterns of aqueous solution cast pure PVA, PEG, (PVA–PEG) blend, and (PVA–PEG)–*x* wt % MMT nanocomposites films. Inset shows the enlarged view of 001 reflection peak of MMT in the nanocomposites. [Color figure can be viewed in the online issue, which is available at wileyonlinelibrary.com.]

Table I. Bragg's Angle 2θ, Basal Spacing d, Full Width at Half Maximum FWHM, Crystallite Size L, Intensity I, and Expansion of Clay Gallery Width W_{cg} of Aqueous Solution Cast PVA–x wt % MMT Nanocomposite Films

Parameters of 001 reflection peak of MMT				
x wt % MMT	2θ (°)	d (nm)	W_{cg} (nm)	I (counts)
MMT	7.03	1.257	0.297	520
1	5.32	1.659	0.699	12
2	5.23	1.688	0.728	33
3	4.71	1.874	0.914	26
5	5.06	1.745	0.785	55
10	4.61	1.915	0.955	125

Parameters of $10\bar{1}$,101 reflection peak of PVA					
x wt % MMT	2θ (°)	d (nm)	FWHM (rad)	L (nm)	I (counts)
PVA	19.56	0.453	0.0094	15.62	3601
1	19.62	0.452	0.0348	4.22	3074
2	19.53	0.454	0.0341	4.30	3097
3	19.58	0.453	0.0346	4.24	2897
5	19.57	0.453	0.0144	10.18	2889
10	19.57	0.453	0.0333	4.41	2250

$10\bar{1}$,101 crystalline reflection planes of the PVA are found almost independent of MMT concentration (Table I). But the crystallite length L of PVA spherulites has a drop of nearly 11 nm on the addition of 1 wt % MMT in its matrix. Table I also shows that the intensity value corresponding to $10\bar{1}$,101 crystalline peak of PVA for the nanocomposites significantly decreases and becomes relatively more broad initially at 1 wt % MMT, which anomalously decreases with the further increase of MMT

Table II. Bragg's Angle 2θ, Basal Spacing d, Full Width at Half Maximum FWHM, Crystallite Size L, Intensity I, and Expansion of Clay Gallery Width W_{cg} of Aqueous Solution Cast (PVA–PVP)–x wt % MMT Nanocomposite Films

Parameters of 001 reflection peak of MMT				
x wt % MMT	2θ (°)	d (nm)	W_{cg} (nm)	I (counts)
MMT	7.03	1.257	0.297	520
1	5.06	1.745	0.785	7
2	5.13	1.721	0.761	16
3	5.05	1.748	0.788	32
5	4.49	1.966	1.006	34
10	5.44	1.623	0.663	47

Parameters of $10\bar{1}$,101 reflection peak of PVA					
x wt % MMT	2θ (°)	d (nm)	FWHM (rad)	L (nm)	I (counts)
PVA	19.56	0.453	0.0094	15.62	3601
PVA–PVP	19.69	0.450	0.0401	3.66	1651
1	19.97	0.444	0.0339	4.33	1021
2	19.61	0.452	0.0221	6.62	1635
3	19.69	0.450	0.0344	4.27	1179
5	19.61	0.452	0.0346	4.24	1389
10	19.76	0.448	0.0295	4.96	927

Table III. Bragg's Angle 2θ, Basal Spacing d, Full Width at Half Maximum FWHM, Crystallite Size L, Intensity I, and Expansion of Clay Gallery Width W_{cg} of Aqueous Solution Cast (PVA–PEO)–x wt % MMT Nanocomposite Films

Parameters of 001 reflection peak of MMT				
x wt % MMT	2θ (°)	d (nm)	W_{cg} (nm)	I (counts)
MMT	7.03	1.257	0.297	520
1	5.06	1.745	0.785	45
2	4.84	1.824	0.864	141
3	4.97	1.776	0.816	167
5	5.04	1.751	0.791	236
10	4.84	1.824	0.864	1030

Parameters of concerted $10\bar{1}$,101 reflection peak of PVA and 120 reflection peak of PEO					
x wt % MMT	2θ (°)	d (nm)	FWHM (rad)	L (nm)	I (counts)
PEO	19.03	0.466	0.0044	33.52	15296
PVA	19.56	0.453	0.0094	15.62	3601
PVA-PEO	19.14	0.463	0.0057	25.65	6614
1	19.23	0.461	0.0226	6.47	2757
2	19.16	0.462	0.0250	5.86	2868
3	19.16	0.462	0.0070	20.72	3161
5	19.68	0.450	0.0340	4.31	2018
10	19.39	0.457	0.0353	4.15	1598
Parameters of 112,032 reflection peak of PEO					
PEO	23.22	0.383	0.0132	11.18	9515
PVA-PEO	23.32	0.381	0.0131	11.23	3939
1	23.36	0.380	0.0127	11.63	1440
2	23.27	0.381	0.0117	12.56	1244
3	23.28	0.381	0.0129	11.40	2060
5	23.42	0.379	0.0137	10.79	303
10	23.17	0.383	0.0102	14.55	351

concentration. This anomalous behavior of the PVA peak intensity values confirms the irregular changes in the PVA and the MMT interactions with the change of the nanofiller concentration, which also decreases the crystallinity of PVA in the nanocomposites.

(PVA–PVP)–x wt % MMT Nanocomposites

The XRD patterns of (PVA–PVP)–x wt % MMT nanocomposites along with the pure PVA, PVP, and their blend are depicted in Figure 2. The absence of sharp peaks in the XRD pattern of pure PVP confirms its amorphous behavior. The PVP has two broad halos at 12.04° and 22.56°, which are found in agreement with the earlier reported XRD patterns of the pure PVP.[22,79] The blending of an amorphous PVP with the semicrystalline PVA results in broadening of the concerted $10\bar{1}$,101 crystalline reflection peak of PVA which reduces the PVA peak intensity of the blend. This confirms the formation of PVA–PVP miscible blend. The miscibility occurs due to strong hydrogen bond interactions between the functional groups of these polymers (–OH groups of PVA and the C=O groups of PVP). The H-bond interaction compatibility in PVA–PVP blend over the entire composition range has already been confirmed by their dynamic−mechanical, morphology, viscosity, and dielectric investigations.[58,65–67]

The results of PVA–x wt % MMT nanocomposites discussed in previous section establish that the strong interactions between PVA and MMT form the intercalated and exfoliated structures, and the relative amounts of these structures vary anomalously with the change of MMT concentration. But the earlier investigations on the PVP−x wt % MMT nanocomposites confirmed that there was a large adsorption of PVP up to 15 wt % MMT loading which mainly resulted the MMT exfoliated structures.[35,36,38] The PVP adsorption takes place due to strong interaction compatibility between the carbonyl groups C=O of PVP and the hydroxyl groups −OH present on the MMT surfaces. From these outcomes, the structural study of the (PVA–PVP) blend dispersed with MMT nanofiller is interesting.

The inset of Figure 2 shows that the 001 crystalline reflection peaks of MMT are highly defused for the (PVA–PVP)–x wt % MMT nanocomposites. The position of these defused 001 reflection peaks are found towards lower angle side as compared

Table IV. Bragg's Angle 2θ, Basal Spacing d, Full Width at Half Maximum FWHM, Crystallite Size L, Intensity I, and Expansion of Clay Gallery Width W_{cg} of Aqueous Solution Cast (PVA–PEG)–x wt % MMT Nanocomposite Films

Parameters of 001 reflection peak of MMT				
x wt % MMT	2θ (°)	d_{001} (nm)	W_{cg} (nm)	I_{001} (counts)
MMT	7.03	1.257	0.297	520
1	4.79	1.843	0.883	18
2	5.06	1.745	0.785	27
3	5.06	1.745	0.785	39
5	4.95	1.783	0.823	160
10	4.99	1.769	0.809	205

Parameters of concerted $10\bar{1}$,101 reflection peak of PVA and 120 reflection peak of PEG					
x wt % MMT	2θ (°)	d (nm)	FWHM (rad)	L (nm)	I (counts)
PEG	19.50	0.454	0.0056	25.82	4241
PVA	19.56	0.453	0.0094	15.62	3601
PVA-PEG	19.52	0.454	0.0345	4.25	1284
1	19.40	0.457	0.0396	3.70	1665
2	19.56	0.453	0.0365	4.02	1340
3	19.53	0.454	0.0123	11.90	1384
5	19.58	0.453	0.0361	4.06	1182
10	19.48	0.455	0.0319	4.60	1231
Parameters of 112,032 reflection peak of PEG					
PEG	23.64	0.376	0.0137	10.73	6035
PVA-PEG	23.25	0.382	0.0137	10.76	80
1	23.07	0.385	0.0015	94.09	41
2	23.44	0.379	0.0087	16.94	124
3	23.02	0.386	0.0102	14.35	143
5	23.39	0.380	0.0035	41.53	102
10	22.99	0.386	0.0015	94.08	52

with that of the pure MMT which confirms the formation of a little amount of MMT intercalated structures. The relatively large amount of MMT exfoliation in these nanocomposites occurs mainly due to adsorption of miscible PVA–PVP blend on the MMT surfaces.

The position of concerted $10\bar{1}$,101 reflection peak of the PVA for the PVA–PVP blend and its nanocomposites with MMT are found slightly at higher angle side as compared with that of the pure PVA (Table II), which results a small decrease in basal d-spacing of the PVA spherulite. The crystallite length L values of the spherulites of PVA–PVP blend and also their nanocomposites are found significantly low as compared with that of the pure PVA. This result is an evidence of the damage of PVA spherulite size due to its simultaneous interactions with the PVP and the MMT in their nanocomposites. The intensity values of $10\bar{1}$,101 reflection peak of PVA spherulite have a large decrease for the PVA–PVP blend, which confirms the relative increase of the amorphous phase of the blend. Table II also shows that the PVA–PVP blend based nanocomposites have an anomalous changes in the intensity values of $10\bar{1}$,101 crystalline peak with the increase of MMT nanofiller concentration.

(PVA–PEO)–x wt % MMT Nanocomposites

The PVA and PEO are semicrystalline polymers, and the blend of these polymers has less molecular interaction compatibility.[68] But the presence of inorganic nanofillers in their blend bridges the polymers molecules and forms the composites.[70,76,77] The investigations on nanocomposites of the PVA and PEO with MMT have established the formation of the intercalated and exfoliated structures.[25,26,30,40] But due to the linear chain structure of PEO and the strong interactions of its ether oxygen atoms with the Na^+ ions present in the MMT galleries form a large amount of PEO–MMT intercalated structures.[40–43,80–82] Therefore, the study of PVA−PEO blend nanocomposites dispersed with MMT has both the academic and technological interest in regards to the confirmation of the relative crystallinity changes of the PVA and PEO spherulites, and also the amount of intercalated MMT structures.

The XRD pattern of pure PEO has major peaks at 19.03° and 23.22° (Figure 3) which are attributed to its 120 and concerted 112,032 reflection planes,[20,80–82] whereas the pure PVA has only one crystalline peak at 19.56° corresponding to the combined effect of its $10\bar{1}$ and 101 crystalline reflection planes. It is found

that both the major peaks of PEO are relatively sharp and have significantly high intensity as compared with the pure PVA (Table III). The crystalline peak position of PVA is very close to the 120 peak of PEO. Therefore the peak appeared at 19.14° for the PVA–PEO blend has been resulted by the combined effect of the 120 reflection peak of PEO and the $10\bar{1}$,101 reflection peak of PVA. Figure 3 shows that the intensity of both the crystal reflection peaks of PEO significantly reduces on blending it with PVA, which confirms the formation of some miscible domains of PEO with PVA in their blend. It can be ascribed to the disruption of PVA and PEO spherulites in the blend. But the presence of both the major reflection peaks also reveals the existence of some PEO domains of their own identity in the PVA–PEO blend.

Table III shows that the values of 2θ, d_{001} and W_{cg} corresponding to 001 reflection plane of the MMT infer the nanocomposite behavior of (PVA–PEO)–x wt % MMT material with a significant amount of MMT intercalated structure. The I_{001} values of the MMT for these nanocomposites have an increase with the increase of MMT concentration. The high value of I_{001} at 10 wt % MMT of the nanocomposite confirms a large amount of PVA–PEO blend intercalation in the MMT galleries. As compared with the PVA−x wt % MMT nanocomposites, the large I_{001} values of (PVA−PEO)−x wt % MMT nanocomposites infer that the presence of PEO in the PVA–PEO blend promotes the amount of intercalation. From Table III, it can be seen that the positions of 120 crystalline reflection peak of these nanocomposites are slightly at higher angle side as compared with that of pure PEO, which also have an anomalous behavior with the increase of MMT concentration. The crystallite length L values of pure PEO spherulites corresponding to 120 crystal reflection plane and the PVA crystal reflection plane are 33.52 and 15.62 nm, respectively, and for the PVA–PEO blend it is found in between these values (25.65 nm) (Table III). The L values corresponding to 120 reflection peak of the PEO for (PVA–PEO)–x wt % MMT nanocomposite films are found very low as compared with that of the PVA–PEO blend which reveals that the dispersion of MMT in the PVA–PEO blend matrix largely decreases the sizes of their spherulites. Table III also shows that the d-spacing and the L values corresponding to 112,032 reflection plane of the PEO in these nanocomposites are smaller than that of the pure PEO. The relatively very low intensity values of the major crystal peaks of the PVA–PEO blend based nanocomposites at 5 and 10 wt % MMT loading are also favored by the corresponding large increase of their MMT I_{001} values. This suggests that more amounts of polymers blend intercalate in the MMT galleries due to that there is a large increase of amorphous content of the nanocomposites.

(PVA–PEG)–x wt % MMT Nanocomposites

Earlier investigations on PEG–x wt % MMT have established that the PEG has strong affinity with the MMT charged sheets due to which PEG molecules can easily intercalate into the MMT galleries.[53–55] The expansion of the MMT basal plane spacing d_{001} due to PEG intercalation ranges from 1.23 nm to 1.82 nm. Further, this increase of interlayer gallery width is almost independent of PEG molecular weight and also the preparation methods of the nanocomposites.[53–55] Analogous to these results, the recent XRD study[73] on three different molecular weight PEGs (PEG600, PEG1000, and PEG1500) based nanocomposites also reveals the formation of MMT intercalated structures. The intercalation of these polymers changes the MMT gallery width up to 1.7 nm, and this value is less affected by the PEG molecular weight. More recently,[56] the detailed study on PEG−MMT nanocomposites over the whole mixing range (from very low up to 70 wt % MMT) concludes that the MMT gallery width expansion in the nanocomposites is mostly 0.8 nm, and it is corresponding to the double layers of PEG molecules incorporated into MMT galleries. The double layers structures of intercalated polymers into MMT galleries have the most stable arrangements from steric considerations, which are revealed from the computer simulation studies on polymer-layered silicate nanocomposites.[83] The d_{001} and W_{cg} values, recorded in Table I, confirm that the intercalated structures of PVA−x wt % MMT nanocomposites expand the 001 basal plane spacing of MMT comparable to that of the double layers accommodated PEG−x wt % MMT nanocomposites.[53–56] Therefore, the study of the nanocomposites based on the PVA−PEG blend dispersed with MMT nanofiller has an importance in regards to confirmation of this polymer blend on the crystallization behavior and in the enhancement of their pharmaceutical and technological applications.[71–73]

Figure 4 shows that the XRD pattern of the pristine PEG has major peaks at 19.50° and 23.64°, which are corresponding to its crystal 120 and concerted 112,032 crystalline reflection planes, respectively.[56] This XRD pattern of PEG has good resemblance to that of the PEO as shown in Figure 3, which is owing to the same repeating unit in the backbone of these polymers molecules. But the Bragg's reflection peaks positions of PEG are found slightly at higher angle side, and their intensity values are low as compared with that of the PEO, which reflects the comparative low crystallinity of PEG. Relatively low crystallinity of PEG is expected due to its low melting temperature as compared with PEO. Further, the XRD pattern of PEG recorded in this study is found in agreement with the patterns of the earlier studies.[56,73] Interestingly, the position of 120 reflection peak of PEG is close to that of the concerted $10\bar{1}$,101 reflection peak of PVA (Table IV), and therefore the XRD pattern of PVA–PEG blend has good resemblance with that of the pure PVA. The 112,032 reflection peak of PEG has almost suppressed in the PVA–PEG blend which confirms the formation of complete miscible phase of this blend. The crystal reflection peak intensity of the PVA–PEG blend is also found very low as compared with the intensity values of the crystal peaks of the pure PVA and the PEG. The low intensities of the PVA–PEG blend reflection peaks are attributed to a large reduce in their crystalline phase. This is due to the large range H-bond formation between the functional groups of PEG and PVA molecules, which results in their transient cross-linked structure.

Table IV shows that the decrease of 001 reflection peak position 2θ of the nanocomposites as compared with the pure MMT results in increase of d_{001} and W_{cg} values of the (PVA–PEG)–x wt % MMT nanocomposites. The values of these parameters confirm the formation of intercalated structures. The intensity of 001 peak (I_{001}) shows a gradual increase with the increase of MMT

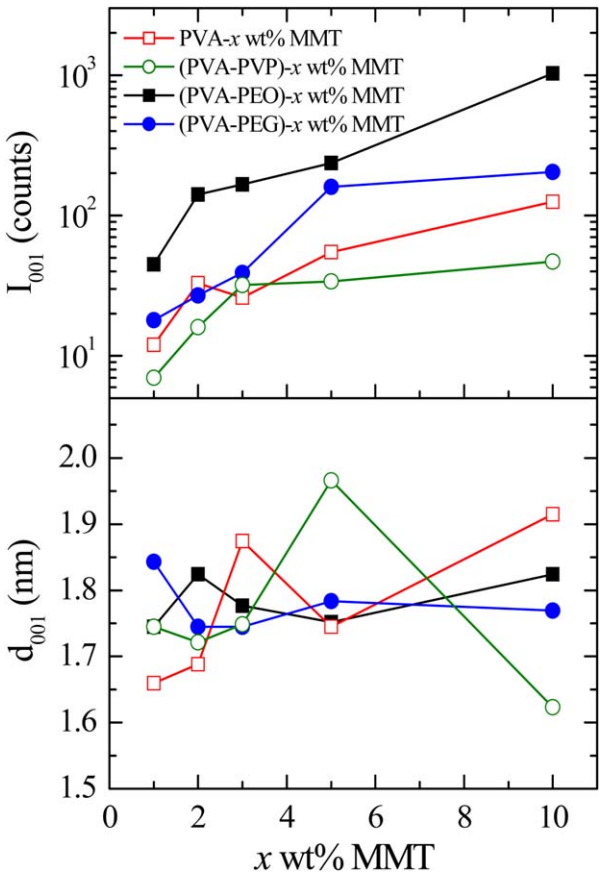

Figure 5. Variation of I_{001} and d_{001} values with MMT concentration of the various nanocomposites. [Color figure can be viewed in the online issue, which is available at wileyonlinelibrary.com.]

loading in the studied nanocomposite which is an evidence of the increase in amount of intercalation. The 2θ values of $10\bar{1}$,101 crystal peak of PVA and also the 112,032 peak of PEG in their blend based nanocomposites have a little change with the increase of MMT concentration. The values of crystallite length L of these nanocomposites corresponding to $10\bar{1}$,101 crystal reflection peak spherulite of PVA are found significantly small as compared with the L values of individual polymer. At 3 wt % MMT loading, the L value is found maximum which suggests the growth in the crystal structure of the blend. Table IV also shows that the intensity values of $10\bar{1}$,101 peak of the nanocomposites have anomalous changes with the increase of MMT concentration in the PVA–PEG blend. A feeble appearance of the 112,032 crystal reflection peak of the PEG and its position at lower Bragg's angle as compared with pure PEG are attributed to a large decomposition of the PEG crystallinity in the presence of MMT. This outcome is in agreement with the earlier results.[53] Table IV shows that the d-spacing of the crystals corresponding to 112,032 reflection peak of PEG for the PVA–PEG blend based nanocomposite has a little variation with the increase of MMT concentration, but there is a drastic variation of the crystallite length L of the spherulites corresponding to this reflection peak.

Figure 5 shows the MMT concentration (x wt % MMT) dependent d_{001} and I_{001} values of different PCNs films. It is found that the d_{001} values have an anomalous variation with the increase of MMT concentration and also with the type of polymers blend in the nanocomposites. This may be due to a variation in the thickness of double layers structures of the intercalated polymer/blends. In case of (PVA–PVP)–x wt % MMT nanocomposites, the d_{001} value is found maximum at 5 wt %, which further decreases significantly at 10 wt %. Although the intercalated amount in this polymer blend is very low, but due to presence of bulky pyrrolidone ring in PVP chain the intercalation of a small amount of PVA–PVP blend results a large increase in d_{001} value at 5 wt %. A large decrease of d_{001} at 10 wt % MMT suggests that some MMT agglomerations are formed due to a large adsorption of the PVA–PVP blend on the MMT surfaces in the nanocomposite. The I_{001} values of all the nanocomposites have a non-linear increase with the increase of MMT concentration, and these values are found relatively high for the (PVA–PEO)–x wt % MMT nanocomposites. The I_{001} values have the order (PVA–PEO)–x wt % MMT > (PVA–PEG)–x wt % MMT > PVA–x wt % MMT > (PVA–PVP)–x wt % MMT. This relative order of the I_{001} values reveals that the blend of amorphous PVP and semicrystalline PVA has low amount of intercalation, whereas the blends of semicrystalline PEO or PEG with PVA have relative high amount of MMT intercalated structures. Further, the presence of bigger size pyrrolidone ring in the PVP backbone hinders its intercalation in the MMT galleries at low MMT concentration in the nanocomposites.

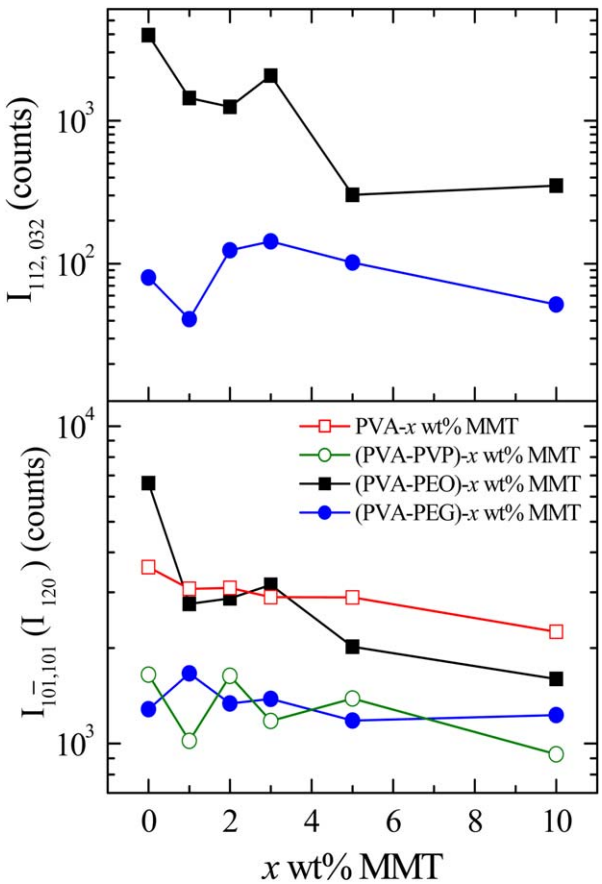

Figure 6. Variation of intensity $I_{112,032}$ and $I_{10\bar{1},101}$ (I_{120}) values with MMT concentration of the various nanocomposites. [Color figure can be viewed in the online issue, which is available at wileyonlinelibrary.com.]

Figure 6 depicts the variation of peaks intensities of the different sizes spherulites formed in the polymeric nanocomposites with the change of MMT concentration. It is found that the intensity value corresponding to crystalline peak of PVA is high for PVA–*x* wt % MMT and (PVA–PEO)–*x* wt % MMT as compared with that of the (PVA–PVP)–*x* wt % MMT and (PVA–PEG)–*x* wt % MMT nanocomposites. Further, the concerted $10\bar{1}$,101 peak intensity values of PVA for both the (PVA–PVP)–*x* wt % MMT and (PVA–PEG)–*x* wt % MMT nanocomposites are found nearly same, and these values have an anomalous change with the increase of MMT concentration. The intensity values $I_{112,032}$ corresponding to PEO or PEG are found relatively high for the (PVA–PEO)–*x* wt % MMT nanocomposites as compared with the (PVA–PEG)–*x* wt % MMT nanocomposites, which is obviously due to the high intensity of pure PEO crystallite reflection peaks as compared with that of the PEG.

CONCLUSIONS

A series of biodegradable polymers based nanocomposites consisted of PVA, and the blends of PVA–PVP, PVA–PEO, and PVA–PEG with MMT as nanofiller were prepared by aqueous solution casting technique. The detailed structural properties of these nanocomposites were explored by the XRD measurements. Besides a large exfoliation, all these nanocomposites have some amount of intercalated structures for MMT concentrations <5 wt % in the polymers matrices, but significant amount of intercalation is found at 5 and 10 wt % MMT concentration (except PVA–PVP blend based nanocomposites). The intercalated amount is relatively more pronounced for (PVA–PEO)–*x* wt % MMT nanocomposites. The blending of semicrystalline hydrophilic polymers reduces the amount of their crystallinity mainly due to extend of intermolecular hydrogen bond interactions between their functional groups, which further decreases in the nanocomposites owing to the polymers and MMT interactions. For these nanocomposites, the MMT gallery width expansion is found in the range 0.66 to 1 nm, which favors the intercalation of polymers double layers structures into the MMT galleries. This detailed study on structural properties especially the evaluation of the decrease of crystallinity and the formation of intercalated/exfoliated MMT structures with the increase of MMT nanofiller concentration can be the key parameters in the design of new novel solid polymer nanocomposite electrolytes and the other advanced functional materials based on these nanocomposites for technological applications.

ACKNOWLEDGMENTS

Authors are thankful to the Department of Science and Technology, Government of India, New Delhi, for the financial support through various research projects. One of the authors S.C. is thankful to the DST, New Delhi for the award of SERB Fast Track Young Scientist research project No. SR/FTP/PS-013/2012.

REFERENCES

1. Shen, Z.; Simon, G. P.; Cheng, Y. B. *J. Appl. Polym. Sci.* **2004**, *92*, 2101.
2. Tanaka, T.; Montanari, G. C.; Mülhaupt, R. *IEEE Trans. Dielec. Electr. Insul.* **2004**, *11*, 763.
3. Darder, M.; Colilla, M.; Ruiz-Hitzky, E. *Appl. Clay Sci.* **2005**, *28*, 199.
4. Ray, S. S.; Bousmina, M. *Prog. Mater. Sci.* **2005**, *50*, 962.
5. Pavlidou, S.; Papaspyrides, C. D. *Prog. Polym. Sci.* **2008**, *33*, 1119.
6. Kanapitsas, A.; Pissis, P.; Kotsilkova, R. *J. Non-Cryst. Solids* **2002**, *305*, 204.
7. Pinnavaia, T. J.; Beall, G. W. Polymer–Clay Nanocomposites; Wiley: Chichester, **2000**.
8. Rajini, N.; Jappes, J. T. W.; Rajakarunakaran, S.; Prabu, M.; Bennet, C. *J. Appl. Polym. Sci.* **2013**, *129*, 3746.
9. Uğur Kaya, A.; Güner, S.; Esmer, K. *J. Appl. Polym. Sci.* **2014**, *131*, 39907.
10. Nazari, T.; Garmabi, H.; Arefazar, A. *J. Appl. Polym. Sci.* **2012**, *126*, 1637.
11. Huang, G.; Wang, X.; Liang, H.; Ye, Y. *J. Appl. Polym. Sci.* **2012**, *124*, 5037.
12. Utracki, L. A.; Sepehr, M.; Boccaleri, E. *Polym. Adv. Technol.* **2007**, *18*, 1.
13. Paul, D. R.; Robeson, L. M. *Polymer* **2008**, *49*, 3187.
14. Chiu, C. W.; Lin, J. *J. Prog. Polym. Sci.* **2012**, *37*, 406.
15. Fried, J. R. Polymer Science and Technology; Prentice-Hall, Inc., Englewood Cliffs: NJ, **1995**.
16. Choudhary, S.; Sengwa, R. *J. Mater. Chem. Phys.* **2013**, *142*, 172.
17. Manuel Stephan, A.; Prem Kumar, T.; Thomas, S.; Selvin Thomas, P.; Bongiovanni, R.; Nair, J. R.; Angulakshmi, N. *J. Appl. Polym. Sci.* **2012**, *124*, 3245.
18. Ravi, M.; Pavani, Y.; Kumar, K. K.; Bhavani, S.; Sharma, A. K.; Narasimha Rao, V. V. R. *Mater. Chem. Phys.* **2011**, *130*, 442.
19. Money, B. K.; Hariharan, K. J. Swenson, *Solid State Ionics* **2012**, *225*, 346.
20. Ghelichi, M.; Qazvini, N. T.; Jafari, S. H.; Khonakdar, H. A.; Farajollahi, Y.; Scheffler, C. *J. Appl. Polym. Sci.* **2013**, *129*, 1868.
21. Choudhary, S.; Sengwa, R. J. *Ionics* **2011**, *17*, 811.
22. Ramya, C. S.; Selvasekarapandian, S.; Hirankumar, G.; Savitha, T.; Angelo, P. C. *J. Non-Cryst. Solids* **2008**, *354*, 1494.
23. Choudhary, S.; Sengwa, R. J. *Ionics* **2012**, *18*, 379.
24. Bergaya, F.; Theng, B. K. G.; Lagaly, G. Handbook of Clay Science; Elsevier: Amsterdam, The Netherlands, **2006**.
25. Strawhecker, K. E.; Manias, E. *Chem. Mater.* **2000**, *12*, 2943.
26. Strawhecker, K. E.; Manias, E. *Macromolecules* **2001**, *34*, 8475.
27. Yu, Y. H.; Lin, C. Y.; Yeh, J. M.; Lin, W. H. *Polymer* **2003**, *44*, 3553.
28. Ip, K. H.; Stuart, B. H.; Thomas, P. S.; Ray, A. *Polym. Test.* **2011**, *30*, 732.
29. Abraham, T. N.; Siengchin, S.; Ratna, D.; Karger-Kocsis, J. *J. Appl. Polym. Sci.* **2010**, *118*, 1297.
30. Sapalidis, A. A.; Katsaros, F. K.; Steriotis, T. A.; Kanellopoulos, N. K. *J. Appl. Poylm. Sci.* **2012**, *123*, 1812.

31. Sengwa, R. J.; Choudhary, S. *Express Polym. Lett.* **2010**, *4*, 559.
32. Sengwa, R. J.; Choudhary, S.; Sankhla, S. *Express Polym. Lett.* **2008**, *2*, 800.
33. Sengwa, R. J.; Choudhary, S.; Sankhla, S. *Polym. Int.* **2009**, *58*, 781.
34. Hild, A.; Séquaris, J. M.; Narres, H. D.; Schwuger, M. *Colloids Surf. A: Physicochem. Eng. Aspects* **1997**, *123–124*, 515.
35. Güngör, N.; Ece, Ö. I. *Mater. Lett.* **1999**, *39*, 1.
36. Séquaris, J. M.; Hild, A.; Narres, H. D.; Schwuger, M. J. *J. Colloids Interface Sci.* **2000**, *230*, 73.
37. Torn, L. H.; Keizer, A.; Koopal, L. K.; Lyklema, J. *J. Colloids Interface Sci.* **2003**, *260*, 1.
38. Koo, C. M.; Ham, H. T.; Choi, M. H.; Kim, S. O.; Chung, I. *J. Polymer* **2003**, *44*, 681.
39. Lombardo, P. C.; Poli, A. L.; Neumann, M. G.; Machado, D. S.; Schmitt, C. C. *J. Appl. Polym. Sci.* **2013**, *127*, 3687.
40. Shen, Z.; Simon, G. P.; Cheng, Y. B. *Eur. Polym. J.* **2003**, *39*, 1917.
41. Chaiko, D. J. *Chem. Mater.* **2003**, *15*, 1105.
42. Elmahdy, M. M.; Chrissopoulou, K.; Afratis, A.; Floudas, G.; Anastasiadis, S. H. *Macromolecules* **2006**, *39*, 5170.
43. Miwa, Y.; Drews, A. R.; Schlick, S. *Macromolecules* **2008**, *41*, 4701.
44. Sengwa, R. J.; Sankhla, S.; Choudhary, S. *Colloid Polym. Sci.* **2009**, *287*, 1013.
45. Sengwa, R. J.; Choudhary, S. *J. Macromol. Sci. Part B: Phys.* **2011**, *50*, 1313.
46. Sengwa, R. J.; Choudhary, S. *Bull. Mater. Sci.* **2012**, *35*, 19.
47. Choudhary, S.; Sengwa, R. J. *J. Appl. Polym. Sci.* **2012**, *124*, 4847.
48. Aranda, P.; Mosqueda, Y.; Pérez-Cappe, E.; Ruiz-Hitzky, E. *J. Polym. Sci. Part B: Polym. Phys.* **2003**, *41*, 3249.
49. Chen, H. W.; Chang, F. C. *Polymer* **2001**, *42*, 9763.
50. Toth, R.; Voorn, D. J.; Handgraaf, J. W.; Fraaije, J. G. E. M.; Fermeglia, M.; Priel, S.; Posocco, P. *Macromolecules* **2009**, *42*, 8260.
51. Sengwa, R. J.; Choudhary, S.; Sankhla, S. *Colloids Surf. A: Physicochem. Eng. Aspects* **2009**, *336*, 79.
52. Chen, B.; Evans, J. R. G.; Holding, S. *J. Appl. Polym. Sci.* **2004**, *94*, 548.
53. Chen, B.; Evans, J. R. G. *Polym. Int.* **2005**, *54*, 807.
54. Chen, B.; Evans, J. R. G. *J. Phys. Chem. B* **2004**, *108*, 14986.
55. Tunney, J. J.; Detellier, C. *Chem. Mater.* **1996**, *8*, 927.
56. Zhu, S.; Chen, J.; Li, H.; Cao, Y. *Appl. Surf. Sci.* **2013**, *264*, 500.
57. El-Houssing, A. S.; Ward, A. A. M.; Mansour, S. H.; Abd-El-Messieh, S. L. *J. Appl. Polym. Sci.* **2012**, *124*, 3879.
58. Cassu, S. N.; Felisberti, M. I. *Polymer* **1999**, *40*, 4845.
59. Abdelrazek, E. M.; Elashmawi, I. S.; Labeeb, S. *Physica B* **2010**, *405*, 2021.
60. Sengwa, R. J.; Sankhla, S. *Polymer* **2007**, *48*, 2737.
61. Ma, R.; Xiong, D.; Miao, F.; Zhang, J.; Peng, Y. *Mater. Sci. Eng. C* **2009**, *29*, 1979.
62. Hill, D. J. T.; Whittaker, A. K.; *Zainuddin. Radiat. Phys. Chem.* **2011**, *80*, 213.
63. Qiao, J.; Fu, J.; Lin, R.; Ma, J.; Liu, J. *Polymer* **2010**, *51*, 4850.
64. Subba Reddy, C. V.; Han, X.; Zhu, Q. Y.; Mai, L. Q.; Chen, W. *Microelectron. Eng.* **2006**, *83*, 281.
65. Rajeswari, N.; Selvasekarapandian, S.; Karthikeyan, S.; Prabu, M.; Hirankumar, G.; Nithya, H.; Sanjeeviraja, C. *J. Non-Cryst. Solids* **2011**, *357*, 3751.
66. Elashmawi, I. S.; Abdel Baieth, H. E. *Curr. Appl. Phys.* **2012**, *12*, 141.
67. Eisa, W. H.; Abdel-Moneam, Y. K.; Shabaka, A. A.; Hosam, A. E. M. *Spectrochim Acta Part A* **2012**, *95*, 341.
68. Mishra, R.; Rao, K. *J. Solids State Ionics* **1998**, *106*, 113.
69. Yang, C. C.; Lin, S. J. *J. Power Sources* **2002**, *112*, 497.
70. Lee, J.; Bhattacharyya, D.; Easteal, A. J.; Metson, J. B. *Curr. Appl. Phys.* **2008**, *8*, 42.
71. Park, S. J.; Kim, H. A.; Choi, J. B.; Gwon, H. J.; Shin, Y. M.; Lim, Y. M.; Khi, M. S.; Nho, Y. C. *Radiat. Phys. Chem.* **2012**, *81*, 857.
72. Suhrenbrock, L.; Radtke, G.; Knop, K.; Kleinebudde, P. *Int. J. Pharm.* **2011**, *412*, 28.
73. Sarier, N.; Onder, E. *Thermochim. Acta* **2010**, *510*, 113.
74. Sengwa, R. J.; Sankhla, S.; Choudhary, S. *Indian J. Pure Appl. Phys.* **2010**, *48*, 196.
75. Choudhary, S.; Sengwa, R. *J. Indian J. Phys.* **2012**, *86*, 335.
76. Sengwa, R. J.; Choudhary, S.; Sankhla, S. *Indian J. Eng. Mater. Sci.* **2009**, *16*, 395.
77. Sengwa, R. J.; Choudhary, S.; Sankhla, S. *Compos. Sci. Technol.* **2010**, *70*, 1621.
78. Assender, H. E.; Windle, A. H. *Polymer* **1998**, *39*, 4295.
79. Sivaiah, K.; Kumar, K. N.; Naresh, V.; Buddudu, S. *Mater. Sci. Appl.* **2011**, *2*, 1688.
80. Homminga, D.; Goderis, B.; Dolbnya, I.; Reynaers, H.; Groeninckx, G. *Polymer* **2005**, *46*, 11359.
81. Burgaz, E. *Polymer* **2011**, *52*, 5118.
82. Choudhary, S.; Sengwa, R.J. *J. Appl. Polym. Sci.* **2014**, *131*, 39898.
83. Kuppa, V.; Manias, E. *J. Chem. Phys.* **2003**, *118*, 3421.